Physicochemical Properties and Structural Refinement of Strontium-Lead Hydroxyapatites

Béchir Badraoui,[a] Adriana Bigi,*[b] Mongi Debbabi,[a] Massimo Gazzano,[b] Norberto Roveri,[b] and René Thouvenot[c]

Keywords: Hydroxyapatite / X-ray diffraction / IR spectroscopy / ^{31}P MAS NMR / Ionic substitution

Continuous series of solid solutions of strontium and lead apatite $Sr_{(10-x)}Pb_x(PO_4)_6(OH)_2$ ($0 \leq x \leq 10$), synthesized in aqueous media have been investigated by X-ray powder-pattern fitting, ^{31}P MAS NMR and IR spectroscopy. The lattice dimensions and the IR frequencies of the solid solutions vary linearly with the atom% of lead. The results of the Rietveld analysis indicated a clear preference of lead for the M(2) site of the apatitic structure, so that in the samples with low Pb content it is almost exclusively found in the M(2) site. ^{31}P MAS NMR spectra at 162 MHz show a unique isotropic signal at δ_{iso} between +2.9 (SrHA) and −0.7 ppm (PbHA). From the variation of δ_{iso} with the phase composition it appears that ^{31}P shielding in these mixed apatites is essentially governed by the nature of the metal in the M(1) site. The qualitative variation of the chemical shift anisotropy of the PO_4 group agrees with the deviation from ideal T_d symmetry shown by the Rietveld refinement analysis.

Introduction

Hydroxyapatites, $M_{10}(PO_4)_6(OH)_2$, crystallizing in the hexagonal lattice, are known for the bivalent metals M = Ca, Sr, Ba, Cd, and Pb.[1−5] Because of the high stability and flexibility of the apatitic structure, a great number of substitutions, both cationic and anionic are possible. In particular, substitution of the bivalent cations has a great influence on the structural, textural, and physical properties of these materials and justifies the increasing number of studies on this subject, which involves several research and application fields: dental and bone pathologies, bioceramics, luminescence, ionic conduction, water treatment by ionic exchange, catalysis, etc.[6−10]

A major contribution to these studies comes from the results of structural refinements of powder X-ray diffraction patterns (Rietveld methods) and of solid-state NMR spectroscopy investigations, performed at high resolution with magic-angle spinning (MAS NMR). Actually, these two methods are complementary and their combined use represents a powerful tool for investigating the localization of the substituted elements in the apatitic cell, as well as the resulting structural modifications.

The unit cell of stoichiometric crystalline apatite hosts ten cations arranged in two non-equivalent positions: four at the M(1) site aligned in the column, each surrounded by nine oxygen atoms, and six at the M(2) site arranged at the apexes of "staggered" equilateral triangles, each surrounded by seven oxygen atoms.[1,2,10]

Ca-Sr, Ca-Ba, Ca-Cd, and Ca-Pb hydroxyapatites have been widely investigated[11−15] (hereafter MHA and M′-M′′HA indicate pure or mixed-metal hydroxyapatites, respectively). The lattice parameters of these mixed apatites vary linearly with the composition, with the exception of the *c* axis of Pb-CaHA that displays a discontinuity at about 50 atom% of lead. The peculiar variation of the *c*-axis dimension has been ascribed to an inhomogeneous lead distribution in the two non-equivalent cation sites, on the basis of the results of powder pattern structure refinements of Pb-CaHA, which indicate a clear preference of lead for site M(2) of the hydroxyapatite structure.[9]

We have previously applied powder pattern fitting refinements and ^{31}P MAS NMR spectroscopy to the study of Cd-Pb and Cd-Sr systems.[16,17] CdHA and PbHA exhibit just a limited range of solubility; cadmium can replace up to 30% of the lead, whereas lead does not seem to "like" the incorporation into CdHA. The cadmium ion displays a

[a] Laboratoire de Chimie Inorganique et Industrielle, Ecole Nationale d'Ingénieurs de Monastir,
5019 Monastir, Tunisie
[b] Dipartimento di Chimica "G. Ciamician", Università degli Studi, and Istituto per la Sintesi e Fotoreattivita', CNR,
Via Selmi 2, 40126 Bologna, Italy
Fax: (internat.) + 39-051/209-9456
E-mail: bigi@ciam.unibo.it
[c] Laboratoire de Chimie Inorganique et Matériaux Moléculaires, UMR CNRS 7071, case courrier 42, Université Pierre et Marie Curie,
75252 Paris Cedex05, France
Supporting information for this article is available on the WWW under http://www.eurjic.com or from the author.

clear preference for the M(1) site of the apatite structure, in agreement with the shorter metal−metal distances in this site with respect to the M(2) site. On increasing the cadmium content, it begins to fill the M(2) site so that at the highest degree of substitution, two of the four metal ions in the M(1) site are Cd, whereas just one of the six metal ions in the equilateral triangles characteristic of site M(2) is Cd. Also $Sr_{(10-x)}Cd_xHA$ were obtained as a single phase in a limited range of composition ($x \leq 4$). In this system, in comparison with the Cd-Pb one, the relatively small Cd^{2+} ion is almost statistically distributed over both sites.

Here we report the results of a structural (Rietveld method) and spectroscopic (IR and ^{31}P MAS NMR spectroscopy) investigation carried out on strontium-lead hydroxyapatites in the whole range of lead substitution for strontium.

Results

X-ray Analysis

Preliminary structural analysis by X-ray diffraction (XRD) shows that all the samples correspond to pure apatitic phases, whatever the Sr/Pb ratio. This is confirmed by structural Rietveld refinements of six samples where the resulting formulae are: $Sr_{8.9}Pb_{1.1}HA$, $Sr_{6.9}Pb_{3.1}HA$, $Sr_{4.9}Pb_{5.1}HA$, $Sr_{4.0}Pb_{6.0}HA$, $Sr_{2.0}Pb_{8.0}HA$, and $Sr_{1.0}Pb_{9.0}HA$. From now onwards, the samples will be indicated as $Sr_{(10-x)}Pb_xHA$, where x corresponds to the stoichiometry resulting from chemical analysis.

Figure 1 displays the final plot for $Sr_{8.9}Pb_{1.1}HA$ and $Sr_{2.0}Pb_{8.0}HA$ samples, as typical comparisons between the observed and the calculated patterns. The refined structural parameters are reported in Table 1, and the data about cationic distribution are reported in Table 2.

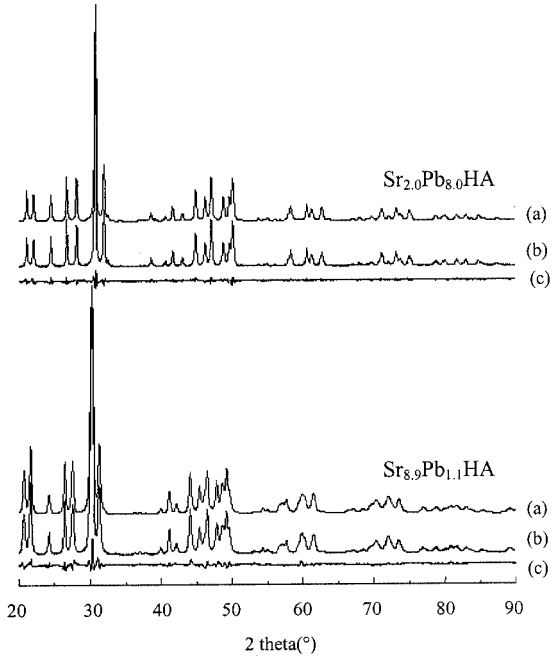

Figure 1. Comparison of the observed [curve (a)] and calculated [curve (b)] powder diffraction patterns of $Sr_{2.0}Pb_{8.0}HA$ and $Sr_{8.9}Pb1_{1.1}HA$ [curve (c)] is the difference profile

The existence of a continuous solid solution between the strontium and lead hydroxyapatite, conforms with the be-

Table 1. Fractional atomic coordinates and equivalent thermal parameters after Rietveld refinement for the mixed Sr-PbHA (e.s.d. in parentheses)

Apatite	Atom	x	y	z	B_{eq} [Å^2]
$Sr_{8.9}Pb_{1.1}$[a]	M(1)	0.3333	0.6667	0.0018(9)	0.6035
	M(2)	0.2438(3)	0.9876(3)	0.2500	0.7214
	P	0.4039(9)	0.3723(7)	0.2500	0.4225
	O(1)	0.338(2)	0.489(2)	0.2500	0.4925
	O(2)	0.583(2)	0.466(2)	0.2500	0.7246
	O(3)	0.347(1)	0.261(1)	0.073(1)	1.2854
	O(H)	0.0000	0.0000	0.325(3)	1.4251
$Sr_{6.9}Pb_{3.1}$[b]	M(1)	0.3333	0.6667	0.0040(1)	0.2351
	M(2)	0.2450(4)	0.9934(5)	0.2500	0.5958
	P	0.4039(6)	0.3726(6)	0.2500	0.9985
	O(1)	0.342(2)	0.498(3)	0.2500	0.5014
	O(2)	0.583(3)	0.470(3)	0.2500	1.009
	O(3)	0.358(2)	0.269(2)	0.073(2)	0.3987
	O(H)	0.0000	0.0000	0.413(6)	1.2514
$Sr_{4.9}Pb_{5.1}$[c]	M(1)	0.3333	0.6667	0.0102(3)	0.3385
	M(2)	0.2482(4)	0.9986(6)	0.2500	0.5924
	P	0.4097(8)	0.3781(5)	0.2500	0.9547
	O(1)	0.340(3)	0.488(3)	0.2500	0.8014
	O(2)	0.596(4)	0.467(3)	0.2500	1.3954
	O(3)	0.359(2)	0.272(2)	0.002(2)	0.5934
	O(H)	0.0000	0.0000	0.444(7)	0.3954
$Sr_{4.0}Pb_{6.0}$[d]	M(1)	0.3333	0.6667	0.0048(8)	0.8210
	M(2)	0.2505(2)	0.0026(8)	0.2500	0.8953
	P	0.4057(2)	0.3698(2)	0.2500	1.4251
	O(1)	0.363(5)	0.474(4)	0.2500	1.8004
	O(2)	0.591(5)	0.464(3)	0.2500	2.1145
	O(3)	0.359(2)	0.268(3)	0.072(2)	1.5926
	O(H)	0.0000	0.0000	0.448(5)	1.2957
$Sr_{2.0}Pb_{8.0}$[e]	M(1)	0.3333	0.6667	0.0055(5)	0.3354
	M(2)	0.2481(4)	0.9987(6)	0.2500	0.8250
	P	0.4029(2)	0.3675(1)	0.2500	0.1687
	O(1)	0.333(3)	0.506(3)	0.2500	0.5140
	O(2)	0.573(3)	0.471(3)	0.2500	0.2954
	O(3)	0.370(2)	0.280(2)	0.084(2)	0.1542
	O(H)	0.0000	0.0000	0.501(5)	0.6982
$Sr_{1.0}Pb_{9.0}$[f]	M(1)	0.3333	0.6667	0.0059(9)	0.5932
	M(2)	0.2517(3)	0.0031(5)	0.250	0.7586
	P	0.4055(2)	0.3744(4)	0.250	1.2476
	O(1)	0.336(3)	0.491(2)	0.250	1.5748
	O(2)	0.578(3)	0.475(3)	0.250	1.9507
	O(3)	0.364(2)	0.276(2)	0.079(2)	1.5842
	O(H)	0.0000	0.0000	0.394(7)	1.1957

[a] a = 9.7736(9) Å, c = 7.2958(4) Å, R_p = 7.2, R_{wp} = 9.2. [b] a = 9.8121(5) Å, c = 7.3203(6) Å, R_p = 6.4, R_{wp} = 8.4. [c] a = 9.8572(7) Å, c = 7.3352(7) Å, R_p = 7.1, R_{wp} = 9.0. [d] a = 9.8625(7) Å, c = 7.3414(8) Å, R_p = 5.6, R_{wp} = 7.8. [e] a = 9.8681(9) Å, c = 7.3616(5) Å, R_p = 7.2, R_{wp} = 9.4. [f] a = 9.8725(8) Å, c = 7.3497(5) Å, R_p = 7.2, R_{wp} = 9.4. The pattern R factor R_p is defined as $R_p = 100\{\Sigma|Y_{oi} - Y_{ci}|/\Sigma Y_{oi}\}$. The weighted pattern R factor R_{wp} is defined as $R_{wp} = 100\{\Sigma W_i(Y_{oi} - Y_{ci})^2/W_i\Sigma(Y_{oi})^2\}^{1/2}$.

Table 2. Lead substitution (atom%) in mixed Sr-PbHA (e.s.d. in parentheses)

	$Pb_1/(Pb_1 + Sr_1)$	$Pb_1/(Pb_1 + Pb_2)$	$Pb_2/(Pb_2 + Sr_2)$	Pb/(Pb + Sr)[a]	Pb/(Pb + Sr)[b]
$Sr_{8.9}Pb_{1.1}HA$	< 1	< 1	14.2(2)	8.6(5)	11.7(2)
$Sr_{6.9}Pb_{3.1}HA$	12.0(1)	15.5(3)	43.5(1)	31.0(4)	31.6(2)
$Sr_{4.9}Pb_{5.1}HA$	30.8(2)	24.0(2)	64.9(2)	51.3(2)	51(2)
$Sr_{4.0}Pb_{6.0}HA$	33.4(1)	21.9(1)	78.9(1)	60.7(1)	60.0(1)
$Sr_{2.0}Pb_{8.0}HA$	58.2(3)	29.2(1)	93.8(1)	79.5(2)	80.0(1)
$Sr_{1.0}Pb_{9.0}HA$	75.6(2)	33.9(2)	98.3(3)	89.3(1)	90.5(2)

[a] Rietveld refinement. [b] Chemical analysis.

havior of Ca-Pb and Ca-Sr apatites.[11,14] The progressive substitution of lead for strontium results in a slight increase in the lattice parameters *a* and *c*; the variation of these sizes is appreciably linear and follows the Vegard law,[18] according to the following relations:

$a = (9.7729 + 0.0122x)$ Å; $\sigma(a) = 9.3 \cdot 10^{-3}$ Å
$c = (7.2761 + 0.0011x)$ Å; $\sigma(c) = 4.7 \cdot 10^{-2}$ Å

Despite this regular variation and the similarity of the ionic radii (coord. 7: Pb^{2+} = 1.37 Å, Sr^{2+} = 1.35 Å; coord. 9: Pb^{2+} = 1.49 Å, Sr^{2+} = 1.45 Å),[19] the variation of the average values of the M(1)−O and M(2)−O distances is someway irregular. In the mixed hydroxyapatites, the phosphate group is considerably distorted by comparison with the limiting phases. A table with M−O distances and distortion indexes is reported as Supporting Information.[20]

According to the similarity of the radii of the two cations the distribution of these ions in both the M(1) and M(2) sites, should be close to a statistical occupancy. However, the refinement shows that the occupancy factor of lead in the M(2) site is always higher than that corresponding to the statistical distribution (Table 3).

Thus, small lead contents (0.86 atom per cell) go almost exclusively into the M(2) site. The difference from the statistical distribution decreases when the lead content increases. We could attribute this behavior, as well as the preferential location of lead in the M(2) site, to the relatively high electronegativity of lead, which increases the polarization of the O−H bond and strengthens the hydrogen bonds, as well as the structural stability of the apatite.[21]

Finally, we observed a good agreement between the values of the Pb/(Pb + Sr) ratios deduced from structural refinements and those obtained by chemical analyses, except for the phase $Sr_{8.9}Pb_{1.1}HA$, which exhibits an appreciably smaller lead incorporation (see Table 2).

Table 3. Statistic distribution and refinement occupancy in the metal M(1) and M(2) sites of Sr-PbHA; the occupancy parameters are normalized to one unit cell content

Pb content [atom/cell]	Refinement distribution (A)		Statistic distribution (B)		(A − B)/B	
	M(1)	M(2)	M(1)	M(2)	M(1)	M(2)
0.86	0	0.86	0.35	0.52	−1.0	+0.65
3.10	0.48	2.62	1.24	1.86	−0.61	+0.41
5.13	1.23	3.90	2.05	3.08	−0.40	+0.27
6.07	1.34	4.73	2.43	3.64	−0.44	+0.30
7.95	2.33	5.62	3.18	4.77	−0.27	+0.18
8.93	3.03	5.90	3.57	5.36	−0.15	+0.10

Infrared Absorption Spectroscopy

The infrared spectra of various mixed apatites show the characteristic absorption bands of the $(PO_4)^{3-}$ groups and OH^- ions of the apatitic structure. Weak bands characteristic of HPO_4^{2-} and CO_3^{2-} ions[22] are also present, as it which can be seen from a typical plot (Figure 2).

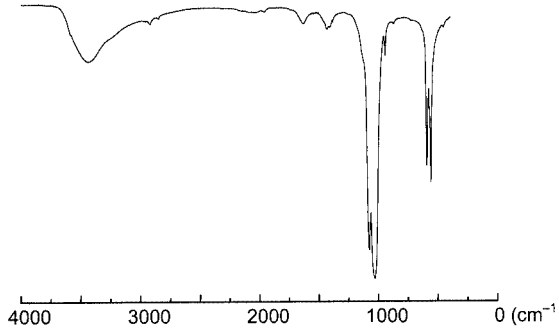

Figure 2. Infrared spectrum of $Sr_{6.9}Pb_{3.1}HA$

The progressive substitution of the lead ions for strontium induces a regular shift of the absorption bands towards smaller wavenumbers as shown in Figure 3.[20]

The shift of the absorption bands of the (PO_4) group can be attributed to the variation of the nature of the metal−oxygen interactions. The character of lead−oxygen interaction is more covalent than that of strontium−oxygen and furthermore a cation of larger mass is involved.[23] The more covalent character of the Pb−OH leads to a shift of the OH vibrational modes towards lower frequency. In particular the shift of the OH stretching mode when the Pb content increases is in agreement with the predominant role of the M−OH interaction with respect to the OH···O(PO_3) hydrogen bond.[24]

^{31}P Solid-State NMR Analysis

Table 4 shows the NMR spectroscopic data for the whole series of mixed Sr-PbHA, as well as that of the pure phases SrHA and PbHA, and Figure 4 shows parts of the 162 MHz MAS spectra obtained at relatively high spinning rates (ca. 5 kHz).

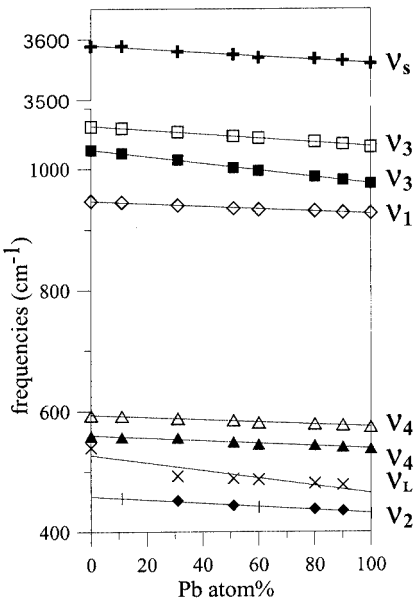

Figure 3. Infrared frequencies of the vibrational modes of strontium-lead hydroxyapatite solid solutions as a function of Pb content; ν_S, ν_L stretching and librational mode of the OH group; ν_1, ν_2, ν_3, ν_4 vibrational mode of the PO_4 group

TAble 4. ^{31}P MAS solid-state NMR spectroscopic data for strontium-lead hydroxyapatites

$Sr_{(10-x)}Pb_xHA$	δ_{iso} [a][b]	$\Delta\nu_{1/2}$ [c]	$\Delta\nu_{static}$ [d]
Sr_{10}	2.9	0.9 (150)	2.6 (16)
$Sr_{8.9}Pb_{1.1}$	3.0	1.2 (200)	2.9 (18)
$Sr_{8.0}$ $Pb_{2.0}$	3.0	1.8 (290)	3.4 (21)
$Sr_{6.9}Pb_{3.1}$	3.0	2.5 (400)	5.3 (33)
$Sr_{6.1}Pb_{3.9}$	3.0	3.0 (490)	8.6 (53)
$Sr_{4.0}Pb_{6.0}$	2.6	4.4 (710)	9.5 (59)
$Sr_{2.8}Pb_{7.2}$	1.9	5.1 (830)	12.3 (76)
$Sr_{2.0}Pb_{8.0}$	0.1	4.8 (780)	6 (37)
$Sr_{1.0}Pb_{9.0}$	−0.7	3.0 (490)	5.1 (31)
Pb_{10}	−0.7	1.2 (190)	3.1 (19)

[a] Position of the central line observed at a high spinning rate (about 5 kHz). [b] In ppm relative to 85% aqueous H_3PO_4 (±0.1 to ±0.2 ppm). [c] In ppm, with the values in Hz in parentheses. [d] Half-height bandwidth of the resonance for non-spinning sample; in kHz, with ppm values in parentheses.

The evolution of the isotropic chemical shift δ_{iso} and of the isotropic full width at half maximum (*fwhm*) as a function of the Pb content is depicted in Figures 5 and 6.

As shown in Figure 4, whatever the phase composition, only one isotropic signal is observed; however, for the samples with relatively high Pb contents, a shoulder is apparent, which cannot be resolved by resolution enhancement. This is not surprising when considering the small chemical shift difference between the limiting phases SrHA (δ_{iso} = +2.9 ppm) and PbHA (δ_{iso} = −0.7 ppm); $\Delta\delta_{iso}$ = 3.6 ppm amounts to only four times the smallest observed line width of SrHA (0.9 ppm, Table 4).

The δ_{iso} variation is far from linear; it does not vary significantly with increasing Pb content up to 60%, where it decreases abruptly, in agreement with a shielding effect of Pb^{2+} compared with Sr^{2+}. This peculiar variation has to be related to the nonstatistical distribution of Pb in both the M(1) and M(2) sites.

The isotropic signal is relatively narrow at low Pb content, it broadens significantly on increasing Pb substitution to reach a maximum value (about 5 ppm) for 70% Pb. This could also be related to the unequal site occupancy, as a

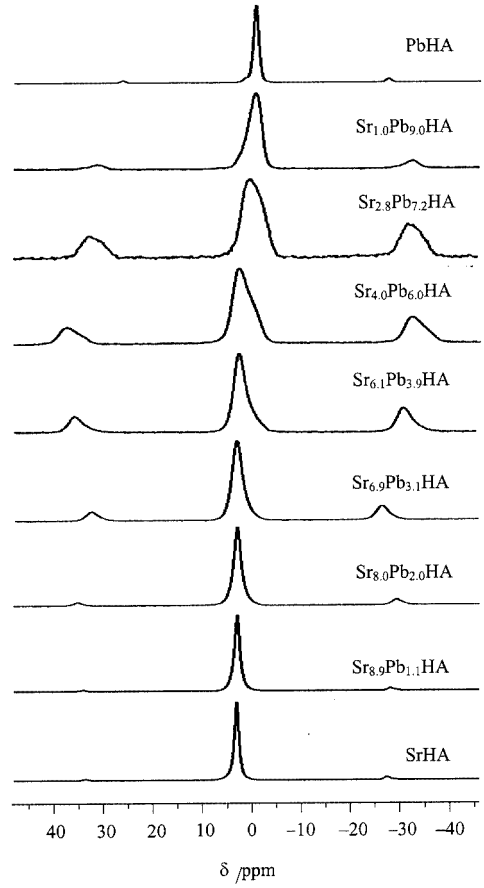

Figure 4. Part of the 162 MHz ^{31}P MAS spectra of the pure and mixed Sr-Pb hydroxyapatites, showing only the isotropic signal and the first (n = +1 and −1) spinning side bands; from bottom to top: SrHA (Ro = 5 kHz, NS = 24), $Sr_{8.9}Pb_{1.1}$ (Ro = 5.1 kHz, NS = 24), Sr_8Pb_2 (Ro = 5.2 kHz, NS = 24), $Sr_{6.9}Pb_{3.1}$ (Ro = 4.9 kHz, NS = 48), $Sr_{6.1}Pb_{3.9}$ (Ro = 5.4 kHz, NS = 48), Sr_4Pb_6 (Ro = 5.6 kHz, NS = 104), $Sr_{2.8}Pb_{7.2}$ (Ro = 5.2 kHz, NS = 72), Sr_1Pb_9 (Ro = 5.2 kHz, NS = 48), PbHA (Ro = 4.3 kHz, NS = 48)

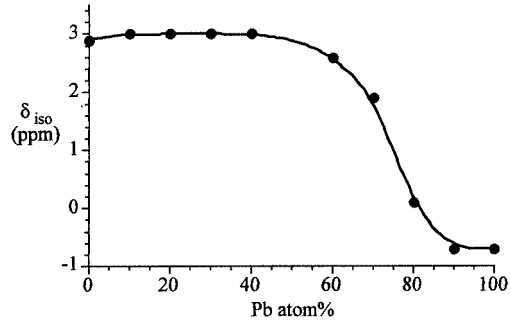

Figure 5. Variation of δ_{iso} as a function of Pb content (atom%)

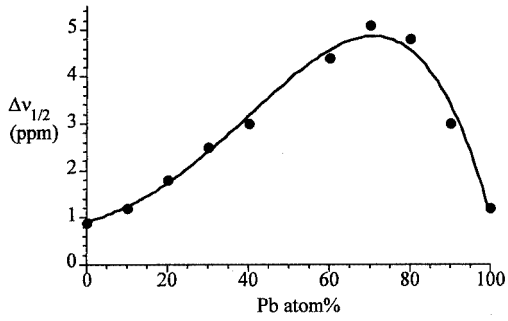

Figure 6. Variation of the full width at half maximum of the isotropic signal as a function of Pb content (atom%)

statistical distribution would have given a symmetrical shape for the $\Delta\nu_{1/2}$ variation.

The chemical shift anisotropy (CSA) of the PO_4 tetrahedron can be derived from the intensity of the spinning side bands (SSB) (see Exp. Sect.). Determination of the chemical shift tensor components and of the CSA is in principle feasible through analysis of the SSB at various spinning rates.[25] However, in the present case, this analysis is virtually impossible because of overlap of numerous unresolved resonances and because of the existence of dipolar interactions which contribute to the SSB intensity at a low spinning rate and significantly broaden the band observed in static spectra.[17] The trend in CSA variation can, however, be qualitatively appreciated from the relative intensity of the first pair of SSB depicted in Figure 4, taking into account that at any fixed spinning rate, the relative intensity of these spinning side bands increases with increasing anisotropy. It is apparent that the CSA of the PO_4 increases smoothly with increasing Pb content, reaching a maximum at around 70% Pb and decreases again with further Pb substitution. This explains the variation of the band width of the static spectra, which, in the absence of any dipolar interaction, would have allowed us a direct determination of the chemical shift anisotropy.

Discussion

The results of this study indicate that SrHA and PbHA form solid solutions over the whole range of composition. Lead substitution for strontium in the hydroxyapatite structure induces a linear expansion of the lattice constants in agreement with its slightly greater ionic radius. Furthermore, Pb is a soft acid and displays a greater tendency towards covalent interactions and directional bonding, whereas strontium can be considered a hard acid. The more covalent character of Pb−O interactions with respect to Sr−O interactions can be invoked to justify the shift of the infrared OH absorption modes towards lower frequencies when the Pb content increases.[24] The increase of lead content also induces a shift of the absorption bands, characteristic of the phosphate internal modes towards lower frequencies. This might either be due to the different ionic character of the metal or to the different anion−anion distances.[23]

The results of the powder fitting structure refinements indicate a clear preference of lead for the M(2) site of the apatitic structure, so that in the samples of low Pb content it is almost exclusively found in the M(2) site. The preference of lead for the M(2) site is in agreement with its slightly greater dimensions with respect to Sr, since in site M(2) the arrangement of the staggered equilateral triangles allows for the optimization of the packing of larger ions, in contrast to the M(1) site where the strict alignment in the columns causes a stronger repulsion. However, a contribution of the more covalent character of the M−O interaction to the cation site preference cannot be excluded, as suggested by the previous results obtained for Sr-Cd apatites[17] where cadmium displays a slight preference for the M(2) site in spite of its small dimensions which should have preferred the hexacoordination of site M(1). A clear preference of Pb for the M(2) site of the apatitic structure was previously reported on the basis of the results of the powder fitting refinements carried out on Ca-Pb apatites.[14] When substituting for calcium, lead almost exclusively fills the M(2) site, until, at Pb contents greater than 45%, it begins to fill the M(1) site, leading to a nonlinear variation of the *c* axis of the apatite structure. The ionic radii and the characters of the metal−oxygen interaction are not as different for Sr and Pb as they are for Ca and Pb. This can account for the minor modifications provoked by lead incorporation into the SrHA structure.

The preference of lead for the M(2) site becomes less evident on increasing the lead content of the solid phase. In agreement, the broadening of the NMR isotropic signal is quite small for the samples at low Pb content and increases when lead is more statistical distributed in the two cationic sites.

Numerous studies, experimental and theoretical, have shown that, among other effects, ^{31}P shielding in phosphate compounds increases − that is δ decreases − with increasing π-bond order between phosphorus and oxygen (p_π-d_π overlap) leading to shorter P−O distances.[26−31]

The shielding effect for pure PbHA (δ = −0.7 ppm) with respect to pure SrHA (δ = 2.9 ppm) can be correlated with the shortening of the mean P−O bond, which decreases from 1.54 Å in SrHA to 1.46 Å in PbHA (Table 1 in Supporting Information[20]).

For the mixed phases we have to consider the various cationic environments of the P atom, that is $PSr_{(9-y)}Pb_y$ (y = 0−9).[16,17] The isotropic resonance of each $PSr_{(9-y)}Pb_y$ environment should be observed between δ = +2.9 (PSr_9 in SrHA) and −0.7 (PPb_9 in PbHA), the shielding increasing with *y*. Accordingly, as we have already discussed for cadmium-lead hydroxyapatites,[16] the incidence in the ^{31}P MAS spectra of the progressive Pb for Sr substitution would have been in the case of a statistical distribution:

− a regular shielding of the isotropic resonance according to δ_{iso} (ppm) = [2.9·(10 − x) − 0.7·x]/10.

− a pseudo-Gaussian shape for the variation of the isotropic *fwhm*, with a maximum at $x = 5$.

On the contrary, both curves (Figures 5 and 6) present singularities for $x = 6-8$. Departure from the theoretical behavior can be accounted for by the results of the Rietveld analysis. At low Pb content, Pb is located almost exclusively in the M(2) site, this means that Sr almost exclusively occupies the M(1) site. The quasi invariance of δ_{iso} for SrPbHA up to 40% Pb could be the indication that in these series the shielding of the ^{31}P nucleus is primarily determined by the nature of the metal in M(1) and consequently influenced very little by the metal in the M(2) site. As can be seen in Table 2, more than 70% of the M(1) sites are occupied by Sr, for Pb contents of up to 60%. Therefore, the singularities observed for both δ_{iso} and $\Delta\nu_{iso}$ curves for around 60−80% Pb could easily be explained if we assume the predominant contribution of the metal in the M(1) site to the ^{31}P shielding.

Let us return to the variation of the chemical shift anisotropy, which reflects the distortion of the PO_4 tetrahedron. For the pure phases SrHA and PbHA, the geometry of the phosphate anion is quite regular and corresponds to a quasi T_d local symmetry with nearly identical P−O distances and all O−P−O angles approaching 109.47°. This explains the low intensity of the spinning side bands (Figure 4) characteristic of a small CSA. For the mixed hydroxyapatites, deviation from the T_d symmetry is evidenced by unequal bond lengths [DI(PO) > 1%] and bond angles [O−P−O between 102 and 116°, DI(O−P−O) up to 5%]. Maximal distortion occurs effectively for the mixed apatites with Pb contents around 60−80% [DI(O−P−O) ca. 0.04−0.05] which actually exhibit the largest chemical shift anisotropy (Figure 4, Table 4).

Experimental Section

Synthesis: The mixed strontium and lead hydroxyapatites with various Pb/(Pb + Sr) ratios, were obtained from a double decomposition method, in aqueous medium.[32,33] Concentrations of the solutions in lead, strontium and phosphate ions correspond to the stoichiometry of the desired apatite. 0.03 M ammonium dihydrogen phosphate [$(NH_4)H_2(PO_4)$, Merck 99%] solution (A solution) and a solution containing a mixture of lead acetate [$Pb(CH_3COO)_2{\cdot}3H_2O$, Fluka 99%] and strontium nitrate [$Sr(NO_3)_2$, Riedel−de Haën AG 98%], with a total concentration of metal cations of 0.05 M (B solution) were prepared. Solution (A) was added dropwise to solution (B), at boiling temperature under a nitrogen stream. The pH value of the slurry was maintained at approximately 12 by regular additions of small amounts of ammonia (Prolabo, $d = 0.89$; 28% aqueous solution). The resulting solid phase was kept in contact with the mother solution for 1 h, at boiling temperature. The precipitate was then filtered, washed with hot distilled water, in order to eliminate traces of ammonium, nitrate and acetate ions, dried at 100 °C for 12 h and calcined at 600 °C for 4 h to improve its crystallinity. Several B solutions, with lead cation fractions ranging from 0 to 1, were prepared and the procedure was repeated in order to obtain the mixed apatites. The compounds obtained were submitted for XRD, chemical analysis, IR spectroscopy, and ^{31}P MAS NMR spectroscopy analyses.

Characterizations: The XRD data were collected with a Philips PW1710 diffractometer, equipped with a copper anode and a graphite monochromator in the diffracted beam ($K_{\alpha 1}$ radiation, $\lambda = 1.5406$ Å). The investigated range was from 18 to 99.99° (2θ), with a step of 0.03° and a counting time of 13 s for each step. The FT-IR spectra (4000−400 cm^{-1}) were recorded with a Bio-Rad FTS 6000 spectrophotometer. 1 mg of the samples was crushed with 300 mg of KBr, and pelletized at 8 tons. The NMR experiments were performed on powdered samples at room temperature with a Bruker MSL400 spectrometer (9.4 T) operating at 162 MHz. A Doty probehead, equipped with 4-mm diameter rotors, was used for spinning rates of up to 6.5 kHz. The spinning rate was monitored by a Bruker pneumatic unit, allowing the control of bearing and drive-inlet nitrogen pressure. Because of unexpected failure of the spinning ratemeter, it was impossible to select and lock a precise spinning rate for all samples; however, bearing and drive pressures were sufficiently stable to avoid fluctuations in the spinning rate. Actually, by comparison with the isotropic signal, no significant broadening of the spinning side bands could be detected and the exact spinning rate was easily determined from the spacing of the spinning side bands. The spectra were acquired using a simple one-pulse sequence with phase cycling (CYCLOPS sequence). Pulse duration was 1 μs that corresponds to a 15° flip angle. The spectral width was 45 kHz (280 ppm). Preacquisition and interpulse delays were 22 μs and 5 s, respectively. The number of transients (NS) was chosen between 24 and about 1000, to obtain a good signal-to-noise ratio, depending on the spinning rate and of the linewidth of the signal. The 4 K free induction decay was zero-filled to the size of 8 K and Fourier-transformed after exponential multiplication of the free induction decay using a 20-Hz line-broadening factor: the final digital resolution of the real spectrum was 10 Hz (0.07 ppm). Chemical shifts are reported with respect to external 85% H_3PO_4 in the IUPAC convention, i.e. positive δ corresponds to a resonance at higher frequency (deshielding) than the reference. Chemical shift values are given with a precision ranging between ±0.1 ppm (narrow resonances) and ±0.2 ppm (broad resonances). The lead and strontium contents in the samples were determined with a Perkin−Elmer 3110 atomic absorption spectrophotometer. The phosphate ions were quantified by visible absorption spectrophotometry of the phosphovanadomolybdic complex. The measurement of the optical densities was carried out at 430 nm.[34] XRD shows that all the samples correspond to pure apatitic phases; according to the results of the chemical analyses the samples exhibit the following formulae: $Sr_{10}(PO_4)_6(OH)_2$, $Sr_{8.9}Pb_{1.1}(PO_4)_6(OH)_2$, $Sr_{8.0}Pb_{2.0}(PO_4)_6(OH)_2$, $Sr_{6.9}Pb_{3.1}(PO_4)_6(OH)_2$, $Sr_{6.1}Pb_{3.9}(PO_4)_6(OH)_2$, $Sr_{4.9}Pb_{5.1}(PO_4)_6(OH)_2$, $Sr_{4.0}Pb_{6.0}(PO_4)_6(OH)_2$, $Sr_{2.8}Pb_{7.2}(PO_4)_6(OH)_2$, $Sr_{2.0}Pb_{8.0}(PO_4)_6(OH)_2$, $Sr_{1.0}Pb_{9.0}(PO_4)_6(OH)_2$, $Pb_{10}(PO_4)_6(OH)_2$.

Structural Analysis: Rietveld full-profile refinements[35] of the mixed strontium-lead hydroxyapatites were carried out by means of the DBWS-9411 program.[36] The space group ($P6_3/m$, no. 176), the cell parameters, the atomic positions and the Debye−Waller factors of SrHA are introduced as the initial structural model for the hydroxyapatite with the lowest lead content. A five-order polynomial was used to simulate the background, while the peaks were fitted using a "pseudo-Voigt" function. Half width of the diffraction peaks as a function of 2θ was evaluated by the formulation of the Caglioti model.[37] Rietveld refinement was performed in several stages, the parameters obtained in each stage being deferred as follows. In the first cycles the scale factor and the background were refined. Refinement of the other parameters was in the following order: profile parameters, zero shift, asymmetry parameter and cell parameters. Refinement of the occupancy factors was done only

for Pb^{2+} and Sr^{2+} ions, with the assumption that these two cations were, initially, statistically located in the two cationic sites, the total contents answering to the stoichiometry obtained by chemical analysis. The apatitic structure comprises 7 independent atoms, corresponding to 21 atomic coordinates, 8 being fixed according to symmetry rules. The other 13 coordinates were refined, starting with those of the two metal sites. In the last refinement cycles, all 30 parameters were released. Then, the refined parameters were used like the initial model for apatite with the lead content immediately higher, and so on. Atomic positions, anisotropic thermal parameters, lattice parameters, reliability pattern factor R_p and weighted factor R_{wp} are gathered in Table 1. A Table in the Supporting Information[20] gives interatomic distances and distortion indices of the phosphate tetrahedron.[38] Lead ion distribution between the two metal sites and chemical analysis results are gathered in Table 3. Equivalent thermal parameters $B_{eq} = \sum_i \sum_j \beta_{ij} (\vec{a}.\vec{b})$ are calculated by the relation: $B_{eq} = 4 \cdot (a^2\beta_{11} + b^2\beta_{22} + c^2\beta_{33} + ab\beta_{12} \cdot \cos(\gamma)/3$.[4] A table with distances, angles and distortion indexes in Sr-PbHA is reported as Supporting Information.[20] Further details of the crystal-structure investigations may be obtained from the Fachinformationszentrum Karlsruhe, 76344 Eggenstein-Leopoldshafen, Germany on quoting the depository numbers CSD-412026 to -412031.

Acknowledgments

We gratefully acknowledge financial support from MURST (Italy), the University of Bologna (Funds for Selected Topics), the Direction Générale de la Recherche Scientifique et Technique (Tunisie) and the Centre National de la Recherche Scientifique (France). NMR measurements were performed at the NMR facility center (SIARE) of the Université Pierre et Marie Curie (Paris).

[1] M. I. Kay, R. A. Young, A. S. Posner, *Nature* **1964**, *204*, 1050−1052.
[2] K. Sudarsanan, R. A. Young, *Acta Crystallogr., Sect. B* **1972**, *28*, 3668−3670.
[3] O. S. Bondareva, Yu. A. Malinkovskii, *Kristallografija* **1986**, *31*, 233−236.
[4] M. Hata, K. Okada, S. Iwai, *Acta Crystallogr., Sect. B* **1978**, *34*, 3062−3064.
[5] S. Brückner, G. Lusvardi, L. Menabue, M. Saladini, *Inorg. Chim. Acta* **1995**, *236*, 209−212.
[6] P. Fourman, P. Royer, *Calcium et tissu osseux − Biologie et pathologie*, Flammarion, Paris, **1970**.
[7] T. Suzuki, Y. Hayakawa, *Proceedings of the 1st International Congress on Phosphorus Compounds*, Rabat, October 17−21, **1977**, p. 381−385.
[8] Y. Matsumura, S. Sugiyama, H. J. B. Hayashi, J. B. Moffat, *J. Solid State Chem.* **1995**, *114*, 138−145.
[9] *CRC Handbook of Bioactive Ceramics*, vol. II ("Calcium Phosphates and Hydroxyapatites Ceramics") (Eds.: T. Yamamuro, L. L. Hench, J. Wilson), CRC Press, Boca Raton, **1990**.
[10] J. C. Elliott, *Structure and Chemistry of the Apatites and Others Calcium Orthophosphates*, Elsevier Sci., The Netherlands, **1994**.
[11] I. Khattech, Degree Thesis, Univeristé de Tunis,Tunisie, **1996**.
[12] A. Bigi, E. Foresti, F. Marchetti, A. Ripamonti, N. Roveri, *J. Chem. Soc., Dalton Trans.* **1984**, 1091−1093.
[13] M. Gazzano, PhD Thesis, University of Bologna, Bologna, Italy, **1986**.
[14] A. Bigi, A. Ripamonti, S. Brückner, M. Gazzano, N. Roveri, S. A. Thomas, *Acta Crystallogr., Sect. B* **1989**, *45*, 247−251.
[15] A. Nounah, J. Szilagyi, J. L. LaCut, *Ann. Chim. Fr.* **1990**, *15*, 409−419.
[16] B. Badraoui, A. Bigi, M. Debbabi, M. Gazzano, N. Roveri, R. Thouvenot, *Eur. J. Inorg. Chem.* **2001**, *5*, 1261−1267.
[17] B. Badraoui, R. Thouvenot, M. Debbabi, *C. R. Hebd. Acad. Sc. Ser. IIC* **2000**, *3*, 107−112.
[18] L. Vegard, *Z. Physik* **1922**, *9*, 395−396.
[19] R. D. Shannon, *Acta Crystallogr., Sect. A* **1976**, *32*, 751−767.
[20] Tables given as Supporting Information (see footnote on the first page of this article).
[21] K. C. Blakeslee, A. Robert, S. R. Condrate, *J. Am. Ceram. Soc.* **1971**, *54*, 559−563.
[22] G. Engel, W. E. Klee, *J. Solid State Chem.* **1972**, *5*, 28−34.
[23] B. O. Fowler, *Inorg. Chem.* **1974**, *13*, 207−213.
[24] M. Andres-Verges, F. J. Higes-Rolando, C. Valenzuela-Calahorro, P. F. Gonzales-Diaz, *Spectrochimica Acta* **1983**, *39A*, 1077−1082.
[25] J. Herzfeld, A. E. Berger, *J. Chem. Phys.* **1980**, *73*, 6021−6030.
[26] J. H. Lechter, J. R. Van Wazer, *J. Chem. Phys.* **1965**, *44*, 815−829.
[27] A. J. R. Costello, T. Gloneck, J. R. Van Wazer, *Inorg. Chem.* **1976**, *15*, 972−974.
[28] A. R. Grimmer, *Spectrochim. Acta* **1978**, *34A*, 941.
[29] A. K. Cheetham, N. J. Clayden, C. M. Dobson, R. J. B. Jakeman, *J. Chem. Soc., Chem. Commun.* **1986**, 195−197.
[30] S. Un, M. P. Klein, *J. Am. Chem. Soc.* **1989**, *111*, 5119−5124.
[31] S. Aime, G. Digilio, R. Gobetto, A. Bigi, A. Ripamonti, N. Roveri, *Inorg. Chem.* **1996**, *35*, 149−154.
[32] A. Bigi, M. Gazzano, A. Ripamonti, E. Foresti, N. Roveri, *J. Chem. Soc., Dalton Trans.* **1986**, 241−244.
[33] A. Bigi, G. Falini, E. Foresti, M. Gazzano, A. Ripamonti, N. Roveri, *J. Inorg. Biochem.* **1993**, *49*, 69−78.
[34] K. P. Quinlan, M. A. De Sesa, *Anal. Chem.* **1955**, *27*, 1626−1629.
[35] H. M. Rietveld, *J. Appl. Crystallogr.* **1969**, *2*, 65−71.
[36] R. A. Young, *J. Appl. Crystallogr.* **1995**, *28*, 366−367.
[37] G. Caglioti, A. Paoletti, F. P. Ricci, *Nucl. Instrum.* **1958**, *3*, 223−228.
[38] W. H. Baur, *Acta Crystallogr., Sect. B* **1974**, *30*, 1195−1215.

Received September 19, 2001
[I01369]